

Dynamics of Architecturally Engineered All-Polymer Nanocomposites

Erkan Senses,^{*,†,‡,¶,||} Madhusudan Tyagi,^{†,‡} Madeleine Pasco,[§] and Antonio Faraone^{*,†,||}

[†]NIST Center for Neutron Research, National Institute of Standards and Technology, Gaithersburg, Maryland 20899-8562 United States

[‡]Department of Materials Science and Engineering, University of Maryland, College Park, Maryland 20742-2115, United States

[¶]Department of Chemical and Biological Engineering, Koc University, Rumelifeneri Yolu, 34450, Sariyer, Istanbul, Turkey

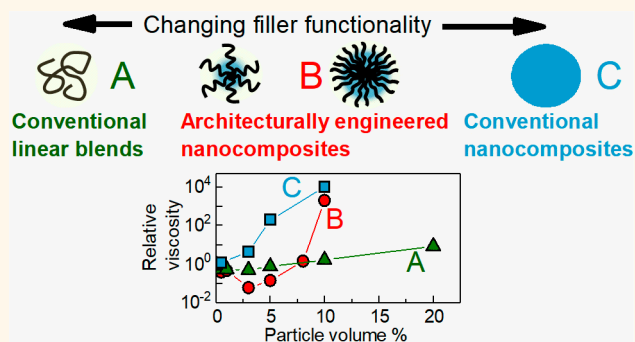
[§]Department of Biology, Rose-Hulman Institute of Technology, Terre Haute, Indiana 47803, United States

Supporting Information

ABSTRACT: We present nanocomposite materials formed by using glassy star-shaped polymers as nanofillers and dispersing them in soft matrices. The resulting “architecturally engineered” polymer nanocomposites structurally reside between the linear homopolymer blends and the conventional polymer nanocomposites with inorganic fillers, inducing reinforcement, which can be as strong as that of solid nanoparticles, or softening depending on the compactness and concentration of the nanoparticles. Such behavior can be traced back to the dynamical features at the local segmental and the chain level, which we investigated using neutron scattering over a wide range of time and length scales in the glassy and melt states of the nanocomposites.

The local and segmental dynamics as well as the degree of chain–chain entanglements are all modified by the star-shaped fillers. The presented approach to tuning the physical properties of all-polymer-based nanocomposites is readily adaptable to other polymer architectures with immediate applications in numerous areas including gas separation membranes, tissue engineering, drug delivery, and functional coatings.

KEYWORDS: polymer architecture, soft nanoparticles, nanocomposites, polymer blends, neutron scattering, rheology



In the search for soft materials with exceptional properties and functionalities, polymer–nanoparticle systems offer great potential.^{1–3} In conventional polymer nanocomposites (PNCs), the unusual viscoelastic behavior results from a number of interconnecting factors, such as particle size,^{4–6} shape,^{7,8} dispersion state,^{9,10} attraction between polymer and particles,¹¹ and, more importantly, topological interactions (entanglements) between the polymer chains in the bulk and the chains interfacing the nanoparticles.¹² Modifying the dynamics within this “interphase” layer can potentially result in advanced responsive materials suitable for changing environments in living and synthetic systems.^{13–17} With conventional choice of rigid nanoparticles and homopolymer, however, this is an extremely challenging task because the dynamics is often determined by the surface–polymer interaction and the particle dispersion states that are hardly altered in solvent-free melt and glassy states. Since the entanglements strongly depend on conformation, engineering the topology within the interphases of nanocomposites could be an alternative route, which we present in this Article.

The advances in synthetic chemistry have now made it possible to precisely control the topology of polymers, which determines many of their physical properties.^{18,19} Rings, stars, combs, bottlebrushes, and hyperbranched polymers have emerged with distinct properties due to their distinct structural and relaxation behavior compared to simple linear polymers.^{20–23} Among them, the star-shaped polymers, in which many linear chains share a common center, are particularly interesting in the present context as the monomer density toward the center increases dramatically at high functionalities, making that part (if not all) of a star macromolecule dense and impenetrable. Depending on the number and the length of arms, they can exhibit both soft/interpenetrable and hard/compact sphere character^{21,24} (see Figure 1, left). We hypothesized that using high- T_g star-shaped polymers as nanofillers and dispersing them in miscible low- T_g linear matrices would create a type of polymer nanocomposite in which the interphases, and therefore

Received: April 4, 2018

Accepted: October 9, 2018

Published: October 9, 2018

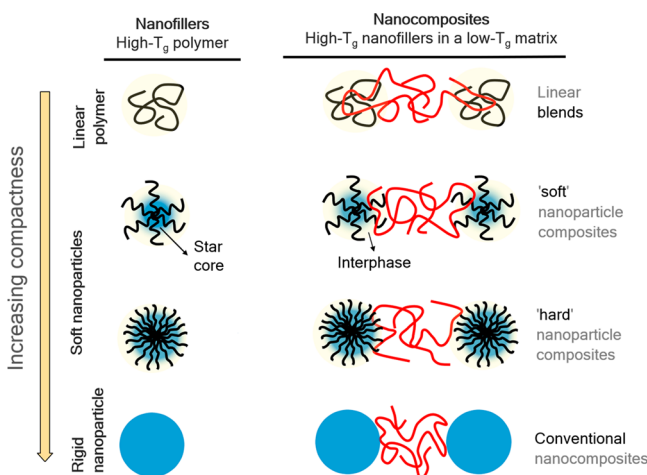


Figure 1. Transition from linear blends to conventional polymer nanoparticle composites. Schematic representation of the architectural engineering of polymer nanocomposites. Increasing functionality of stars leads to a denser core region that is impervious to the matrix chains and gives rise to a more particle-like nature.

the bulk rheological properties, can be systematically varied through macromolecular architecture. As the structural properties of stars vary from soft to hard colloids, the resulting nanocomposites transition from the well-known simple linear blends to hard sphere–polymer nanocomposites (see schematics in Figure 1). In this work, we investigate this scenario through a series of elastic modulus measurements in this transition regime on various samples differing in the molecular weight and functionality of the dispersed high- T_g polymer. Moreover, static and quasielastic neutron scattering measurements allow exploring the nanoscopic structural and dynamical features within the nanocomposites. The nanoscopic dynamical features manifest at the macroscopic level by causing marginal viscosity increases in composites with loose stars or linear blends, whereas the compact, “nanoparticle”-like star polymers cause a decrease in viscosity at low volume fractions while reinforcing the nanocomposites at high concentrations as strongly as can be achieved using silica nanoparticles at the same volume fraction. The demonstrated influence of filler architecture on the rheological properties can be used for tuning nanocomposite properties *via* architectural engineering of polymeric fillers.

RESULTS AND DISCUSSIONS

To create the nanocomposites, we primarily used polystyrene (PS, $T_{g,PS,bulk} \approx 373$ K) as fillers and poly(vinyl methyl ether) (PVME, $T_{g,PVME,bulk} \approx 245$ K) as matrix (detailed sample preparation protocols are given in the Methods section). This system is known to be miscible up to at least 423 K,^{25,26} and the components exhibit a very large difference in T_g s; therefore, their

linear mixtures have been commonly referred as “dynamically asymmetric”.^{27–29} While the star–linear blends of the same chemistry (exhibiting similar dynamical behaviors) have been studied previously,^{30,31} the structure and relaxation of dynamically asymmetric star–linear blends are not known.

Nanostructure. We first studied the conformation and dispersion of PS fillers (20% by mass) in the PVME matrices using small-angle neutron scattering (SANS) (the detailed specifications of the PS linear and star polymers are given in Table 1). We use a deuterated PS (dPS) and hydrogenated PVME (hPVME, 22 kg/mol) matrix to get a coherent intensity in SANS (Figure 2a). At short length scales ($Q \gtrsim 0.2 \text{ \AA}^{-1}$), all

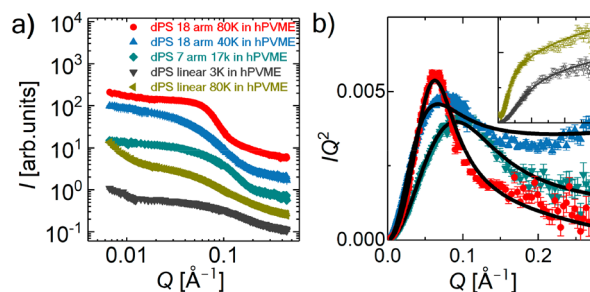


Figure 2. Conformation of PS in the PVME matrix. (a) Small-angle neutron scattering on dPS in the hPVME matrix shows the nanoscale structural differences between linear and star dPS in hPVME. The intensities are shifted vertically for ease of comparison. (b) Kratky plots (*i.e.*, IQ^2 vs Q) after subtracting the incoherent background reveal strong intrachain correlation peaks in the star dPS, a feature absent for linear dPS, which instead shows the usual Gaussian conformation. The lines represent the best fits using random phase approximation with the star polymer (for $f = 7$ and $f = 18$) form factors with the excluded volume parameter and Debye form factor of linear PVME matrix chains (see Supporting Information for details). The same legend of plot (a) applies to plot (b), as well.

profiles display $I \sim Q^{-2}$ scaling, typical for a Gaussian conformation described by the Debye form factor. The filler architecture is manifest in the intermediate length scales where the Q -dependence of the intensity in the star composites shows well-defined peaks in the Kratky plots, IQ^2 vs Q (Figure 2b). This is a clear structural indication of the compact—“nanoparticle-like”—nature of the star polymers.^{32,33} The peaks get narrower and move to larger length scales with increasing number of arms due to denser core regions. Such intrastar peaks are not observed in the linear dPS particles in hPVME (the insets of Figure 2b), suggesting the loose structure of linear PS is retained in the blends. The low- Q upturn in the sample with linear 80 kg/mol PS is due to interpenetrating linear chains at 20 vol %, resulting in a Lorentz contribution to the overall scattering at low- Q . Such an upturn is not seen in the star-polymer fillers, signifying good dispersion of the PS particles in the PVME matrix. Detailed

Table 1. Molar Masses, Arm Radius of Gyration in PVME (Obtained from SANS), Hydrodynamic Size in Toluene (Obtained from DLS), and Calorimetric Glass Transition Temperatures of PS Particles

polymer	M_w , total (kg/mol)	D_{total}	M_w , arm (kg/mol)	D_{arm}	$\langle R_g \rangle_{arm}$ (nm)	$\langle R_h \rangle$ (nm)	$T_{g,DSC}$ (K)
dPS linear-S	3.5	1.05	1.75	1.05	1.69 ± 0.13	NA	353.9 ± 2.6
dPS linear-L	80	1.05	40	1.05	2.62 ± 0.13	7.79 ± 0.11	375.9 ± 3.0
dPS 7 arms	19	1.23	2.6	1.25	1.36 ± 0.19	2.74 ± 0.35	354.3 ± 3.5
dPS 18 arms-S	46.5	1.99	2.6	1.73	3.06 ± 0.17	7.26 ± 0.69	364.3 ± 6.9
dPS 18 arms-L	88	1.10	4.8	1.15	3.26 ± 0.04	5.43 ± 0.08	364.9 ± 2.9

analysis of the SANS profiles reveals the conformation and sizes of the star polymers in the matrix (see [Supporting Information](#) and [Table 1](#)).

The linear PS–linear PVME system is known to be an LCST type, miscible below 423 K,^{25,26} however, the phase behavior of the star PS–linear PVME system has not been explored. We, therefore, performed SANS experiments on the composites with the highest functionality star (18-arm dPS (80 kg/mol) in hPVME at elevated temperatures up to 423 K) to confirm the miscibility of the star PS–PVME (see [Supporting Information](#)), where we performed neutron scattering experiments.

Thermal and Rheological Properties. The structure of star polymers with uneven monomer density and chain ends along the radial direction³⁴ greatly influences their glass transition. We first look at the neat dPS fillers in the absence of a PVME matrix; their DSC traces are displayed in [Figure S3](#), and the obtained T_g values are listed in [Table 1](#).

Blending the PS fillers with the low- T_g PVME matrix at the fixed PS volume fraction of 20% causes elevated yet highly broadened T_g ([Figure 3b](#) and [Table S1](#)) due to the presence of dynamical heterogeneities inherent to the system. For dynamically asymmetric polymer blends, the T_g of the soft component (in this case PVME) is less affected by blending with the high- T_g component due to connectivity of the chains that leads to a self-concentration effect shown by Lodge and

McLeish.³⁵ In our composites, the T_g shifts remain within 10 K, consistent with the earlier reports on the linear PS–PVME blends,^{29,36–38} and are seemingly independent of filler architecture within the uncertainties of the measurements (see [Supporting Information](#) for the values and additional discussion).

Despite marginal effects of filler architecture on the composite glass transition, the consequences on the macroscopic rheology are significant. [Figure 3b](#) compares the linear elastic moduli (see [Supporting Information](#) for viscous component) of the hPVME composites with 18-arm star (88 kg/mol total), seven-arm star (19 kg/mol total), and linear (80 and 3 kg/mol) dPS fillers. The linear, entangling, PS increased the elastic moduli of the composites (at low frequency) about 3 orders of magnitude relative to the neat matrix due to its loose interpenetrating structure that forms its own rigid network in the soft matrix. On the other hand, the reinforcing effect of 18-arm star PS was 2 orders of magnitude smaller due to its highly compact, impenetrable nature. Being less compact, however, seven-arm PS caused an increase in elastic modulus of about 2 orders of magnitude (similar to that caused by short PS chains), which is located between that of linear entangling and 18-arm PS stars.

In the conventional nanocomposites with inorganic fillers, the mechanical reinforcement is often explained in terms of concentration- and dispersion-dependent nanoparticle percolation,^{9,10} change in polymer mobility due to attractive polymer–nanoparticle interactions,¹¹ and entanglements within the interphases of polymer and the nanoparticles.¹² Since the PS particles in each of our nanocomposite samples were 20%, that is, below the percolation threshold of hard spheres (31 vol %),³⁹ and the particles are well-dispersed, the variation of the elastic moduli over a range of 3 orders of magnitude at the same particle concentration is clearly a consequence of the filler architecture.

Such an effect on the rheology is intriguing, as it offers an original way to engineer nanocomposites for desired/optimized properties; however, a thorough understanding of the microscopic mechanisms is essential and will be the focus next. High-resolution neutron spectroscopy on isotopically labeled particles in nanocomposites allows directly observing the chain motions at the nanoscale by simultaneously accessing a broad range of time scales (from sub-nanoseconds to a hundred nanoseconds) and length scales (from monomer size to entanglement mesh sizes). Specifically important for polymers are the localized fast dynamics on the sub-monomer level, the segmental dynamics at the monomer level, and the entangled/collective dynamics at larger scales. Since the nanocomposite properties are predominantly determined by the dynamics of the matrix chains and also the PS fillers are essentially frozen in the time scale of the neutron experiments (see also [Supporting Information](#) for details), we exclusively focus on the dynamics of the PVME matrix chains for the microscopic dynamics described below.

Localized Sub- T_g Dynamics. We first studied the nanoscale dynamics of hPVME linear chains in the presence of dPS with different architectures using a high-flux neutron backscattering instrument (HFBS). The scattering intensity is dominated by the self-motion of H atoms in the PVME at time scales ranging from 100 ps to ~ 1 ns and the momentum exchanged wavevector (Q) range relevant to segmental motions above T_g . The temperature scan of the elastic scattered intensity gives a general picture of the motions and dynamic transitions taking place in the samples. Within the instrumental resolution, only the dynamics slower than ~ 1 ns contribute to the elastic

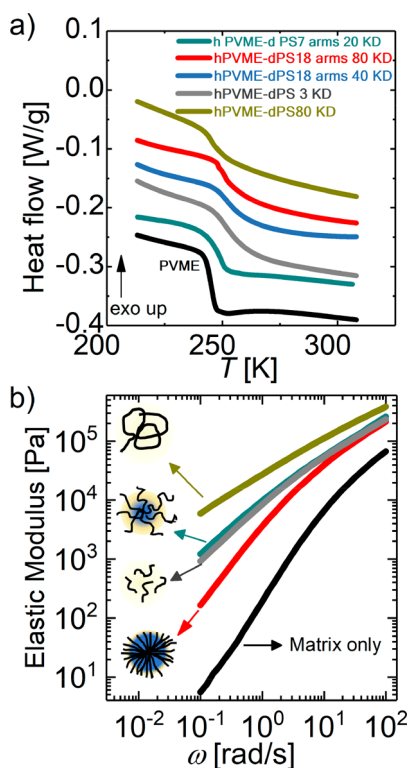


Figure 3. Bulk thermal behavior and rheology of the nanocomposites. (a) Differential scanning calorimetry (DSC) traces showing the glass transition temperature (T_g) of the composites with hPVME and the blends of 80% hPVME matrix and 20% dPS fillers. (b) Linear elastic moduli for the neat PVME, PVME–PS linear (3 and 80 kg/mol), and PVME–PS star (18 arms, 88 kg/mol, and 7 arms, 19 kg/mol) composite samples at the same 20% loading show the variation over 3 orders of magnitude with less reinforcing effect of the compact highly functionalized star particle. The same legend of plot (a) applies to plot (b), as well.

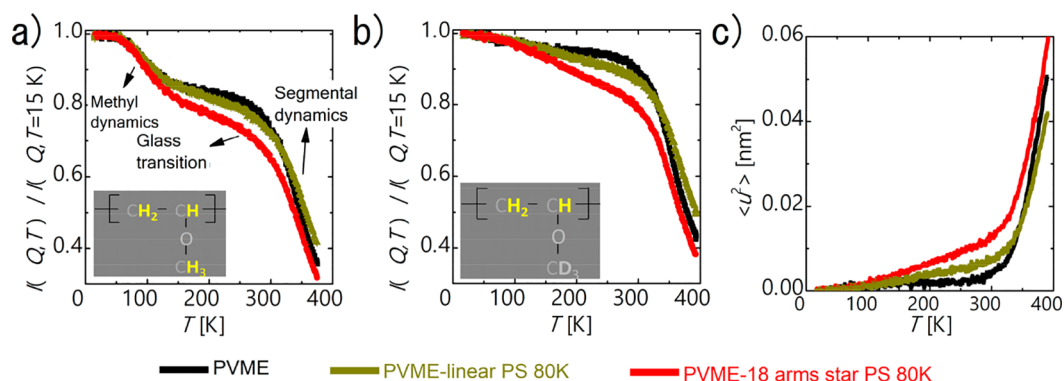


Figure 4. Elastic intensity temperature scans. Normalized scattered elastic intensities of PVME in neat forms and in composites with 20% linear (80 kg/mol) and 18-arm (88 kg/mol) deuterated PS. Motions faster than ~ 1 ns are not detected and, therefore, cause a decrease of the elastic intensity. The PVME in (a) is fully hydrogenated, whereas in (b) the methyl groups of PVME are deuterated and, therefore, made invisible to the scattering (also shown in the insets). (c) Mean-square displacements of H atoms on partially deuterated PVME chains in the nanocomposites; notice the enhanced glassy dynamics along with a clear broadening of the segmental dynamics activation near T_g in the samples with dispersed PS stars.

intensity, while faster processes cause a decrease in the elastic intensity. The elastic intensities were normalized to those obtained at the lowest temperature ($I_{el}(Q,T)/I_{el}(Q,T=15\text{ K})$) to eliminate specimen size dependence of the scattering and allow a meaningful comparison between the samples. Elastic neutron scan measurements can probe the mean square displacement of hydrogen atoms even below the glass transition temperature.⁴⁰ Above the glass transition, the observed motions can be related to the Rouse segmental dynamics of the polymer; below the glass transition local motions of the hydrogen atoms trapped in a harmonic or soft potential are probed. These latter dynamical processes can be relaxational or vibrational in character and are distinct from the Rouse segmental dynamics probed above the glass transition.

Figure 4a displays the normalized elastic intensities summed over all Q (0.25 to 1.75 \AA^{-1}) for the neat hPVME and hPVME blends with linear dPS and 18-arm-star dPS of similar total molecular weights (~ 80 kg/mol) (see Supporting Information for other PS particles). All data superimpose up to 50 K, where the first stepwise decrease of the intensity is observed due to the methyl group rotation⁴¹ dynamics exiting the ~ 1 ns dynamic window. At $T \approx 250$ K, all samples experience a major intensity drop associated with the onset of faster segmental motions of the PVME chains. Note that this temperature is close to the calorimetric T_g of the blend measured in differential scanning calorimetry (DSC) and somewhat independent of the PS architecture.

The neat hPVME and the hPVME with linear PS follow a similar continuous decay up to around 250 K, suggesting that the localized sub- T_g motions are not much affected by blending with linear chains, consistent with previous results.³⁷ At temperatures above T_g , however, the elastic intensity is higher in the presence of linear dPS compared to the neat form, due to slower segmental motions of PVME in the presence of the less mobile linear PS, as observed in binary blends of linear chains.^{32,37}

Interestingly, for PVME in the presence of star-PS, the elastic intensity exhibits a larger decrease as the temperature is increased around and below T_g , indicating accelerated dynamics (with respect to pure PVME) of H atoms in the glassy regime. This is clearly due to the PS architecture and different from linear blends, in which the localized sub- T_g processes remain unaltered. Different dynamical processes might be underlying the observed phenomenon; hence, we performed additional

experiments to better understand the underlying mechanism. The motion of H atoms on PVME consist of fast vibrational motions, methyl group rotations, and translational dynamics due to segmental movements. The segmental motions are effective only at $T > T_g$; therefore, they cannot be associated with the sub- T_g dynamics. To differentiate between the methyl group contribution and the localized segmental motions, we used mixtures of methyl group deuterated PVME and a fully deuterated PVME matrix filled with the same linear and 18-arm dPS particles at the same 20% by mass. In these samples, the contribution from the methyl groups on PVME is eliminated and the elastic intensity is due only to the localized motions of the H atoms in the PVME backbone. Figure 4b shows the temperature scan of the elastic scattering intensity for these samples. Clearly, the stepwise decrease at $T \approx 50$ K seen in the samples with hPVME (Figure 4a) is now eliminated; yet, the faster sub- T_g decay in the star-PS-blended PVME endures. It is, therefore, likely that the fast, localized motions of PVME segments are accelerated by the presence of highly compact star-PS molecules.

More quantitatively, the Q -dependence of the elastic intensity can be related to the mean-square displacements, $\langle u^2 \rangle$, by the equation $I_{el}(Q,T)/I_{el}(Q,T \rightarrow 0) = \exp(-Q^2 \langle u^2 \rangle / 3)$ (Figure 4c). At the same $T = 150$ K, the mean square displacement of PVME in blend with star dPS is $\sim 0.4 \text{ \AA}^2$, which is nearly 2 times larger than that in the neat form and in the linear blend. The previous dielectric relaxation studies clearly showed that the low- T_g chains can locally relax faster in blends with linear high- T_g polymers compared to their neat form due to the dynamic confinement effect of the frozen high- T_g chains. This was attributed to enhanced free volume introduced by blending with linear chains.^{27,29} It is possible that the high- T_g star polymers with a large number of free ends provide even more free volume for the low- T_g component to locally relax faster below the T_g . This is also consistent with the recent dielectric spectroscopy results by Holt *et al.*,⁴² where they reported faster sub- T_g dynamics in nanocomposites with polymer-grafted nanoparticles (akin to highly functionalized star-shaped polymers) compared to the nanocomposites with nanoparticles physically adsorbing polymers due to enhanced free volume within the graft layer.

A direct consequence of such behavior of the local dynamics can be clearly observed on the dynamic fragility, m , which

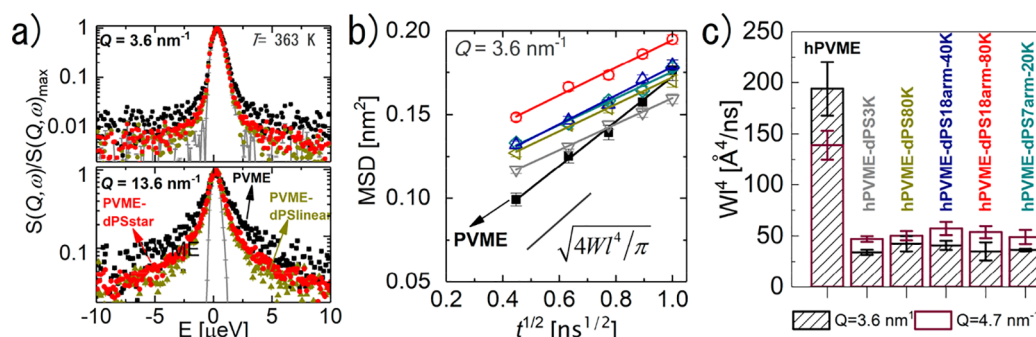


Figure 5. Architectural effects on the segmental dynamics. (a) Normalized dynamic structure factors at 363 K and at representative values of Q , namely, 3.6 and 13.6 nm^{-1} for the neat hPVME, hPVME in 20% linear PS (80 kg/mol), and hPVME with 20% star PS (18 arms, 88 kg/mol). The lines represent the instrumental resolutions determined at $T = 15 \text{ K}$, where all motions are practically frozen. (b) Mean-square displacements (shown at $Q = 3.6 \text{ nm}^{-1}$) determined from the inverse Fourier transformation of the dynamic structure factors into time domain and displayed as a function of $t^{1/2}$ (Rouse scaling). The slopes are directly related to the Rouse parameter, WI^4 , and the obtained values for all samples are displayed in (c). The legend of plot (c) applies to plot (b), as well.

quantifies how far the temperature dependence of the relaxation time of a glass former deviates from the Arrhenius behavior as the T_g is approached from above.⁴³ Qualitatively, the stronger glasses exhibit broader and smoother glass transition. A close look at the elastic intensities around T_g of PVME in Figure 4a and b clearly shows extremely broad transition of PVME in composite with the star PS, suggesting that PVME forms stronger glasses in the presence of stars, in conjunction with an enhanced sub- T_g relaxation. For the composite samples, DSC is conveniently used to determine the dynamic fragility index from the cooling rate dependence of the thermodynamic fictive temperature (see Supporting Information). The dynamic fragility indices were found to be very close for the neat PVME ($m_{\text{PVME}} = 110 \pm 8$) and PVME–linear PS blend ($m_{\text{PVME-PSlinear}} = 88 \pm 11$) within the experimental uncertainties, whereas the fragility of the PVME–star PS composite ($m_{\text{PVME-PSstar}} = 70 \pm 3$) diverges to the strong glass regime.

In short, the filler architecture has a pronounced effect on the fast, localized motions of the matrix chains even in the glassy state. Such architectural influence on the sub- T_g relaxation processes offers a way to optimize the glassy properties of the polymers, such as their fragility and aging.

Segmental Motions. Particularly important for the bulk flow of polymers is the segmental motion that dominates the mobility above T_g . Since the localized motions of PVME segments contribute to the elastic intensity decays at high temperatures as well, the absolute values of $\langle u^2 \rangle$ (or the elastic intensities above T_g in Figure 4) may not be used to directly compare the segmental dynamics.

A more precise comparison was made possible by performing quasielastic neutron scattering (QENS) measurements in a dynamic range of $\pm 11 \mu\text{eV}$ (with a resolution of $0.8 \mu\text{eV}$). At relatively low Q and long times, the molecular details of the chain backbone become unimportant, and the fast, localized motions are not captured. The incoherent dynamic structure factor, $S_{\text{incoh}}(Q, \omega)$, was obtained for samples with hPVME matrices with dPS fillers at 363 K (representative profiles are in Figure 5a) and at 393 K (see Supporting Information). The quasielastic broadening at low Q is, therefore, directly related to the slow, Rouse motion of the chain segments. By Fourier transform and deconvoluting the instrument resolution from the dynamic structure factor, we obtain the self-intermediate scattering function, which is, within the Gaussian approxima-

tion, related to the mean-square displacement of the polymer segments,⁴⁴

$$S_{\text{self}}(Q, t) = \exp[-Q^2/6\langle r^2(t) \rangle] \quad (1)$$

In the Rouse model, the mean square displacements (MSD), $\langle r^2(t) \rangle$, is related to the elementary Rouse rate, WI^4 , by $\langle r^2(t) \rangle = \sqrt{4WI^4t/\pi}$ where $W = 3kT/(\zeta l^2)$ with ζ being the monomeric friction coefficient and l being the segment length.

Figure 5b shows the MSD against $t^{1/2}$ for the neat PVME (black squares) and the PS–PVME composites at $Q = 3.6 \text{ nm}^{-1}$ at 363 K. The linear dependence validates the application of the Rouse model up to 1 ns for this length scale. The slopes of the fitted lines are directly related to the Rouse rates. The obtained numbers of WI^4 for $Q = 3.6$ and 4.7 nm^{-1} are compared in Figure 5c. We have also performed experiments at 393 K on the neat hPVME and the hPVME composites with 18-arm star dPS (80 kg/mol) and linear dPS (80 kg/mol); similar trends were found (see Supporting Information). The segmental dynamics of PVME is clearly slowed down in the presence of PS. The nearly 4-fold decrease of the Rouse parameter of PVME in the composites (at 363 K) compared to its neat form is practically independent of the chain architecture. Such behavior can be attributed to the friction imposed by the PS chains; in fact, at 393 K, above the PS glass transition with lower friction, the PVME Rouse rates decreased only by half upon blending with linear and star PS (the trend is similar within the experimental uncertainties) (see Supporting Information). A previous work by Arbe *et al.*⁴⁵ on a PEO–PMMA blend ($\Delta T_g \approx 200 \text{ K}$) showed that the Rouse dynamics of PEO slowed down in a similar way in its blends with linear and internally cross-linked PMMA at same volume fraction. Our work on the PS–PVME system with various PS architectures put this observation in a more general context: At the segmental level, the entropy-driven Rouse dynamics of the low- T_g component in the polymer blends is tuned by the friction imposed by the essentially frozen high- T_g component, regardless of its molecular architecture. In other words, the monomeric friction coefficient is mainly determined by chemistry rather than the shape of the macromolecules. Thus, the segmental Rouse dynamics is clearly affected by the star architecture in a different way than the localized dynamics is.

Collective Dynamics. In the intermediate time scales, the chains feel the presence of other chains in the melt, and their motion is constrained by entanglements. Such phenomenon directly affects the viscous flow of the system, as the rubbery

plateau modulus is inversely proportional to the square of the entanglement distance. To investigate how the presence of the PS fillers affects the PVME chain dynamics and their entanglements, we used a mixture of a fully deuterated (70%) and a methyl-deuterated (30%) PVME matrix with dPS linear (80 kg/mol) and 18-arm dPS star (88 kg/mol) fillers at the same concentration used for the QENS experiments. By doing this, the scattering intensity at low Q originates from the scattering contrast between the labeled PVME chains and the deuterated matrix, allowing the study of the single-chain dynamics of PVME in the samples. We used neutron spin-echo (NSE), which provides the longest time resolution accessible by any neutron scattering technique, to measure, in the time domain, the normalized intermediate scattering function (ISF), $S(Q,t)/S(Q,0)$, of PVME chains up to 100 ns (at $T = 393$ K).

Figure 6a compares the normalized ISFs using a Q^4t scaling, showing the deviation from the Rouse prediction (shown as

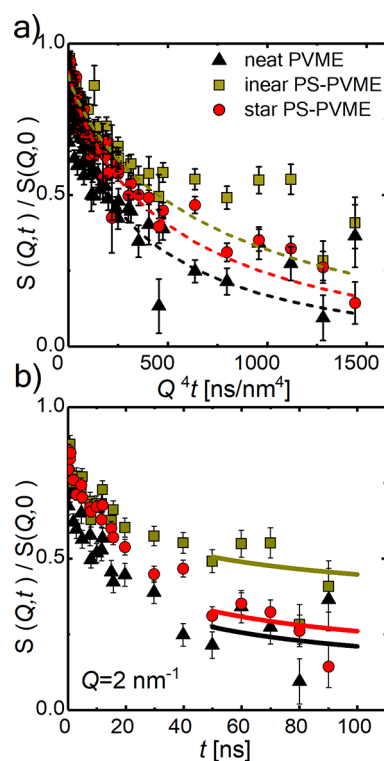


Figure 6. Single-chain dynamics measured by neutron spin-echo. Normalized intermediate scattering functions at $Q = 1.1, 1.5,$ and 2 nm^{-1} and $T = 393$ K of a mixture of deuterated and methyl-hydrogenated PVME (h/d: 15/85), neat, with 20% linear dPS (80 kg/mol), and with 20% star dPS (18 arms, 88 kg/mol). (a) Data shown using a Q^4t Rouse scaling variable. The dashed lines are the decays predicted by unrestricted Rouse motion; the deviations at long times are indicative of confined motion of PVME due to entanglements. (b) Normalized intermediate scattering function at $Q = 2 \text{ nm}^{-1}$ displaying changes in the long-time plateau behavior. The lines are fit to de Gennes formulation for a reptation motion of linear polymers within confining tubes (see the text).

dashed lines; also see Supporting Information) above 500 ns/nm^4 corresponding to $Q = 2 \text{ nm}^{-1}$ and $t > 30$ ns as shown in Figure 4b. It is clearly seen that the neat PVME decays faster in the initial Rouse region, while it is slowed down by the PS fillers, as also observed using QENS. At longer times, a plateau starts to develop associated with the confined motion of PVME chains

due to entanglements. The PVME in the neat form and in composites with star PS have similar plateau levels, while the linear PS shows a significantly enhanced confining effect. The actual values of the confinement tube diameter can be determined by fitting the data to the reptation model formulated by de Gennes:⁴⁶

$$\frac{S(Q, t)}{S(Q, 0)} = \left[1 - \exp\left(-\frac{Q^2 d^2}{36}\right) \right] S^{\text{local}}(Q, t) + \exp\left(-\frac{Q^2 d^2}{36}\right) S^{\text{esc}}(Q, t) \quad (2)$$

where $S^{\text{local}}(Q, t) = \exp(t/\tau_0) \text{erfc}(\sqrt{t/\tau_0})$ describes the local dynamics within the tube with characteristic time scale $\tau_0 = 36/(W^4 Q^4)$. $S^{\text{esc}}(Q, t)$ represents the long-time escaping process of the chain out of its original tube and is not observed in the time scale probed by NSE, and therefore, $S^{\text{esc}}(Q, t) = 1$. The long-time plateau level is determined by $\exp(-Q^2 d^2/36)$, d being the reptation tube diameter. Since the model does not apply for the unrestricted Rouse regimes and we only observe the plateau at $Q = 2 \text{ nm}^{-1}$, we fit the de Gennes equation for this Q value and $t > 50$ ns. We use W^4 values obtained from the fitting to the unrestricted Rouse model of the data shown in Figure 6b (see Supporting Information) and determined the reptation tube diameters in the samples as $d_{\text{PVME-neat}} = 5.63 \pm 0.92 \text{ nm}$, $d_{\text{PVME-dPSstar}} = 4.99 \pm 0.35 \text{ nm}$, and $d_{\text{PVME-dPSlinear}} = 3.45 \pm 0.16 \text{ nm}$. Clearly, the star particles do not much alter the apparent tube size of PVME, whereas blending with linear chains reduces the tube diameter by $\sim 40\%$. The nanoparticle-like star PS fillers, therefore, allow linear PVME chains to move more freely compared to the case of linear blends. This is, indeed, in parallel with our recent observation that the nanoparticles smaller than the entanglement mesh sizes can induce disentanglements of matrix chains by dilating the reptation tube.⁵ The star particles we use in NSE have sizes comparable to the mesh size of the neat PVME; therefore, it is likely that the apparent increase of tube size due to star PS relative to the linear PS is a result of competing effects of geometric confinement, which tends to contract the tube,⁴⁷ and dilation effect of small nanoparticles. The latter is lacking in the case of linear blends; therefore, the tube size decreases.

Let us summarize the dynamical effects of filler compactness and architecture on the matrix chains:

- When the chain segments are considered to be frozen (glassy) at the nanoscopic time scales, the fast, vibration-type localized motions on the chain backbone are greatly accelerated in the presence of compact fillers but remain unaltered in the linear blends or less compact starts.
- In the melt state, the segmental motions are significantly slowed down by addition of high- T_g fillers, but we did not find any effect of filler architecture on the Rouse dynamics, suggesting that the average friction coefficient in nanocomposites is not significantly influenced by the shape of the fillers.
- The collective motion of the linear matrix chains in the presence of nanoparticle-like compact fillers is faster than that of linear blends, as evidenced by the changes in the reptation tube diameters.

Effect of Nanoparticle Concentration. In light of the observed microscopic dynamics, we look into the rheological behavior in more detail. The increase of the effective friction

coefficient, as well as the entangling effect induced by the linear PS chains onto the PVME matrix, and the entanglement between fillers and the matrix chains are all expected to induce significant reinforcing of the composite. On the other hand, star fillers whose sizes are smaller than the reptation tube diameter are expected to disentangle the matrix, therefore inducing a softening effect.⁵ The rheological behavior displayed in Figure 3b on the same filler concentration (20% by volume) clearly shows such competing trends. Since the architecture of the particles had no effect on segmental dynamics, the variation of the elastic moduli comes from the entanglements of the filler macromolecules with the matrix as well as, eventually, with themselves. The most compact filler has the least reinforcement effect, as it behaves like a small nanoparticle⁵ with less ability to entangle with the matrix chains, and allows chains to move more freely.

The reinforcing trends of the different architectures are better seen at different concentrations. Figure 7a shows the effects of

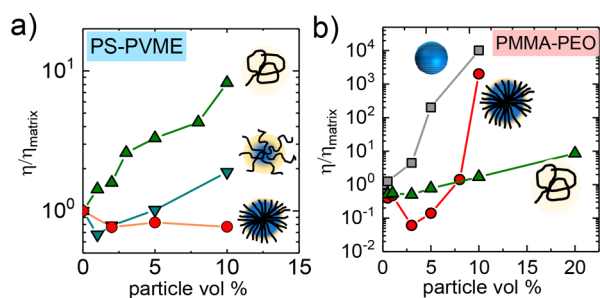


Figure 7. Effect of nanoparticle concentration (% of volume fraction) on the bulk rheology. (a) Viscosities of the star PS–PVME composites with 30 arms, 30 kg/mol (red circles), 8 arms, 40 kg/mol (blue inverted triangles), and 8 arms, 390 kg/mol (green triangles) relative to the viscosity of the neat matrix at 303 K. (b) Comparison of the reinforcing effects of 16-arm PMMA (310 kg/mol), linear PMMA (320 kg/mol), and silica nanoparticles (13 nm diameter) dispersed in a PEO matrix (100 kg/mol) at 393 K. The viscosity numbers are the complex viscosities at $\omega = 0.1$ rad/s.

additional PS-star polymers, namely, 30 arms (30 kg/mol), 8 arms (40 kg/mol), and 8 arms (390 kg/mol) dispersed in PVME matrices at different concentrations (the details of these samples are given in the Supporting Information), on the viscosities of the samples calculated at a deformation frequency of $\omega = 0.1$ rad/s. Eight-arm PS with a total molar mass of 390 kg/mol monotonically increased the viscosity of the composite relative to the neat PVME, similar to the effect of a linear long PS chain. Having a more compact structure with enhanced core region, the 8-arm PS with 10-fold shorter arms exhibited a non-monotonic reinforcing effect. Below 5% loading, the viscosity of this composite sample was remarkably lower than the neat matrix, but became higher upon further increasing the particle loading. Using even higher star functionality (30 arms) with very short arm length, the particle is highly compact and the viscosity of the composite remained lower than the neat matrix up to 10% loading with no indication for mechanical reinforcement. These results suggest that the compactness of the polymeric nanoparticles, which depends on both number of arms and the length of the arms, may be a parameter for controlling rheological properties of the nanocomposites.

To validate our findings beyond the PVME/PS system, we have also studied the architecture effect of poly(methyl methacrylate) (PMMA) on the resulting composites with long

poly(ethylene oxide) (PEO) matrix chains (100 kg/mol) (see Supporting Information for the polymer specifications and sample preparation). This system is known to be miscible up to around 500 K.^{48,49} The role of the PMMA architecture on the bulk rheology is shown in Figure 7b. In the investigated concentration range, linear PMMA only marginally affects the viscosity with monotonic increase with respect to the neat PEO. Star PMMA (16 arms, 320 kg/mol total M_w), however, softens the system at low concentration with an order of magnitude decrease of viscosity as observed in nanocomposites with small gold nanoparticles dispersed in PEO.⁵ Larger viscosity reduction in this system compared to PS–PVME is expected due to a negligibly small enthalpic interaction between PEO and PMMA compared to the small attraction between PS and PVME. Nevertheless, by further increasing the concentration of star PMMA particles, the composite is reinforced over 3 orders of magnitude relative to the neat matrix. The reversing trend after a softening is understood by the overlapping impenetrable glassy PMMA stars at higher loadings, which results in a percolated stiff network within the soft PEO matrix. A similar gel-like transition in star polymer solutions was observed by Loppinet *et al.*⁵⁰ and attributed to jamming of overlapping star polymers; our nanocomposites expand such observation to solvent-free high-modulus systems. While highly compact star macromolecules behave similarly to hard-sphere colloids, the free ends of the stars can still interact with the other star fillers,⁵⁰ either direct arm–arm contact or through the entanglements with the matrix chains; the resulting network formation is highly dependent on the chain architecture. Also, the gradual increase of the viscosity by addition of linear chains suggests that chain interpenetration is not sufficient to observe nanoparticle-like reinforcement; the impenetrable and tunable core region plays a significant role.

Finally, we also prepared bare silica (13 nm diameter) filled PEO composites to make a comparison between architecturally engineered composites to the conventional nanocomposites (Figure 7b). As expected, the hard silica nanoparticles cause a monotonic and 4-fold increase in the viscosity with no softening effect with concentration. The star PMMA–PEO composite shows a similar strong reinforcing trend following strong softening, whereas the linear blend of PMMA and PEO has a marginal effect on the viscosity. This is clearly the result of the nanoparticle-like nature of the star polymers that can be finely tuned by the length and number of arms (Figure 1). It is also noteworthy that the glassy polymer nanoparticles soften at high temperatures above their T_g . To extend the operating temperatures of these nanocomposites, physical and/or chemical cross-linking of the soft nanoparticles may be employed alongside engineering their topology.

CONCLUSIONS

By varying the topology of high- T_g polymers from linear to highly functionalized star polymers and dispersing them in linear soft low- T_g polymer matrices, we presented an approach to designing all-polymer-based nanocomposites where the size and “softness” of the dispersed component are highly tunable. Whereas the chemical nature of the polymers and their interaction affect significantly the segmental mobility through the friction coefficient, the architecture of the high- T_g polymer influences the free volume and hence the fragility of the composite on approaching the glass transition. On the other hand, in conjunction with the dynamic asymmetry,¹⁶ the size of the dispersed particles⁵¹ alters the entanglement of the matrix as well as determines at what concentration the percolation of the

“soft nanoparticles” takes place, which dictates the viscoelastic behavior of the composite at high loadings. In general, these systems show distinct rheological properties compared to conventional polymer–inorganic nanoparticle mixtures and polymer blends. For example, the compact, “nanoparticle”-like star polymers with a large number of short arms exhibit a large viscosity reduction in nanocomposites at low concentrations while also reinforcing the composites at high concentrations, as strongly as inorganic nanoparticles can achieve. This dual effect (softening and stiffening) of filler topology on the rheological properties of these nanocomposites is lacking in the previously explored linear polymer blends and polymer–inorganic nanoparticle mixtures. The presented approach to architectural engineering in nanocomposites can be immediately applied to other polymer shapes, such as dendrimers, bottlebrushes, and rings, to rationally design soft materials with desired properties. Moreover, as the star arms can be synthesized to be of different chemistry and end groups, the demonstrated effect of chain architecture on the viscoelasticity can be readily combined with multifunctionality of star polymers already shown in, for example, nanoelectronics, tissue engineering, drug-targeted delivery, batteries, imaging, antibacterial coatings, and catalysis.^{52,53}

METHODS

Sample Preparation. Fully hydrogenated poly(vinyl methyl ether) (hPVME, 22 kg/mol, $D = 1.09$), methyl deuterated PVME (d3-PVME, 16 kg/mol $D = 1.14$), fully deuterated PVME (d6-PVME, 14 kg/mol $D = 1.15$), and fully deuterated poly(styrene) (dPS, see Table 1 for specifics) were purchased from Polymer Source Inc. hPVME was further dried at 80 °C under vacuum for 2 days and stored at room temperature under vacuum. Toluene (reagent, ACS grade) was supplied from Tylor Scientific and used as received. hPVME and dPS (20% weight fraction in the dry films) were codissolved in toluene at 30 mg/mL by mechanically stirring for 6 h. The solutions were then cast onto aluminum foils with dimensions of approximately 10 cm (L) \times 3 cm (W) \times 3 cm (H) and dried under a fume hood. The dried films were then annealed at 80 °C for 4 days in a vacuum oven and then brought to room temperature and stored in a vacuum until used. Blend samples with the matrix of d3-PVME and dPVME (15/85 ratio) were prepared using the same protocol described. PMMA (Polymer Source Inc.) and silica (Nissan Chemicals America) composites with PEO (Sigma-Aldrich) were prepared using a similar protocol but with chloroform (for PMMA–PEO) and acetonitrile (silica–PEO). The samples were dried and annealed subsequently at 90 °C for 2 days and at 120 °C for 12 h to remove the residual solvents.

Small-Angle Neutron Scattering. SANS was performed on NGB30 at the NIST Center for Neutron Research (NCNR, Gaithersburg, MD, USA). Samples were placed between quartz windows. The measurements were performed at three configurations with sample-to-detector distances of 1, 4, and 13 m and with a neutron wavelength of $\lambda = 6$ Å to cover a Q -range from ~ 0.004 to 0.5 Å⁻¹. All scattering profiles were corrected for background, empty cell, and sample transmission to get 1D isotropic scattering patterns using Igor-based SANS packages⁵⁴ developed by NCNR.

Neutron Backscattering. The fixed window elastic scans and QENS experiments were performed using the NG2-high-flux backscattering spectrometer⁵⁵ at the NCNR. The fixed window elastic scans were run between 15 and 353 K at a heating rate of 1 K/min. The intensity was collected across 16 detectors in a Q -range of 0.25 to 1.75 Å⁻¹, corresponding to length scales of ~ 25.1 to ~ 3.59 Å. The detailed protocol for the QENS experiments was given previously.¹⁶ Briefly, a dynamic range of ± 11 μ eV (with a resolution of 0.8 μ eV full width at half-maximum) was obtained with Doppler-shifted neutrons at a frequency of 15 Hz with incident wavelength of 6.27 Å. Samples were cast on Al foils to obtain a uniform thickness of ~ 100 μ m with $\sim 90\%$ transmission. An annular shape of 3 cm diameter and 3 cm height films

were sealed into an Al can in a He environment. Background subtraction was based on an empty cell, and the detector efficiency was corrected using vanadium data. Resolution for each sample was first obtained at 15 K, and the samples were heated to desired temperature followed by a 1 h thermal equilibration.

Neutron Spin–Echo Spectroscopy. We used a mixture of methyl group deuterated PVME with fully deuterated PVME (at a ratio d3-PVME/d-PVME = 15/85) as a matrix and dPS as the fillers to study single-chain PVME dynamics using the NGA NSE spectrometer at NCNR. The measurements were performed at 393 K using a wavelength of $\lambda = 8$ and 11 Å ($\Delta\lambda/\lambda \approx 0.17$) for Fourier times up to 100 ns and a wave vector range from $Q = 0.11$ to 0.2 Å⁻¹. The samples were sealed in Al cans in a helium environment. Charcoal was used to obtain the NSE instrumental resolution. Both HFBS and NSE data were reduced and analyzed using the software package DAVE.⁵⁶

Thermal Characterizations. The heat capacities of the samples were measured using a DSC (TA Instruments Q 2000). The samples were first heated to 363 K at a 10 K/min rate and maintained there for 5 min. The samples were then cooled to 203 K at a cooling rate of 10 K/min and equilibrated there for 5 min. Finally, the samples were heated to 433 K at a rate of 10 K/min. The glass transition temperatures were identified using the inflection point on the heat flow curve from the last heating ramp.

Mechanical Spectroscopy. Rheology experiments were conducted on a strain-controlled ARES-G2 rheometer (TA Instruments) equipped with 8 mm parallel plates. The frequency sweep measurements were performed in the linear viscoelastic regime at 303 K for PS–PVME and 353 K for PEO–PMMA systems.

ASSOCIATED CONTENT

Supporting Information

The Supporting Information is available free of charge on the ACS Publications website at DOI: 10.1021/acsnano.8b02514.

Supplemental small-angle neutron scattering, glass transition, quasielastic neutron scattering, and neutron spin–echo data (PDF)

AUTHOR INFORMATION

Corresponding Authors

*E-mail: esenses@ku.edu.tr.

*E-mail: antonio.faraone@nist.gov.

ORCID

Erkan Senses: 0000-0003-2593-1146

Antonio Faraone: 0000-0002-3783-5816

Author Contributions

E.S. conceived the idea. E.S. and A.F. designed the experiments. E.S. prepared the samples and performed thermomechanical characterization with help from M.P. E.S., M.T., and A.F. performed the dynamic neutron scattering experiments. E.S. performed the SANS experiments. E.S. and A.F. wrote the manuscript with contributions from M.T. All authors have given approval to the final version of the manuscript.

Notes

The authors declare no competing financial interest.

ACKNOWLEDGMENTS

This work utilized facilities supported in part by the National Science Foundation under Agreement No. DMR-1508249. We thank Dr. Paul Butler for his support on performing the SANS measurements as well as for his valuable review of this paper. We thank Drs. Jack Douglas and Alexandros Chremos for valuable discussions on the glass transition of stars. We are thankful to Drs. Aaron Forster and Ajay Krishnamoorti of The Security Technologies Group at NIST for the use of the rheometer and

calorimeter. Certain tradenames and company products are identified in order to specify adequately the experimental procedure. In no case does such identification imply recommendation or endorsement by the National Institute of Standards and Technology, nor does it imply that the products are necessarily the best for the purpose.

REFERENCES

- (1) Capadona, J. R.; Shanmuganathan, K.; Tyler, D. J.; Rowan, S. J.; Weder, C. Stimuli-Responsive Polymer Nanocomposites Inspired by the Sea Cucumber Dermis. *Science* **2008**, *319*, 1370–1374.
- (2) Shanmuganathan, K.; Capadona, J. R.; Rowan, S. J.; Weder, C. Stimuli-Responsive Mechanically Adaptive Polymer Nanocomposites. *ACS Appl. Mater. Interfaces* **2010**, *2*, 165–174.
- (3) Kumar, S. K.; Benicewicz, B. C.; Vaia, R. A.; Winey, K. I. 50th Anniversary Perspective: Are Polymer Nanocomposites Practical for Applications? *Macromolecules* **2017**, *50*, 714–731.
- (4) Fu, S.-Y.; Feng, X.-Q.; Lauke, B.; Mai, Y.-W. Effects of Particle Size, Particle/Matrix Interface Adhesion and Particle Loading on Mechanical Properties of Particulate–Polymer Composites. *Composites, Part B* **2008**, *39*, 933–961.
- (5) Senses, E.; Ansar, S. M.; Kitchens, C. L.; Mao, Y.; Narayanan, S.; Natarajan, B.; Faraone, A. Small Particle Driven Chain Disentanglements in Polymer Nanocomposites. *Phys. Rev. Lett.* **2017**, *118*, 147801.
- (6) Nusser, K.; Schneider, G. J.; Pyckhout-Hintzen, W.; Richter, D. Viscosity Decrease and Reinforcement in Polymer–Silsesquioxane Composites. *Macromolecules* **2011**, *44*, 7820–7830.
- (7) Zhao, D.; Ge, S.; Senses, E.; Akcora, P.; Jestin, J.; Kumar, S. K. Role of Filler Shape and Connectivity on the Viscoelastic Behavior in Polymer Nanocomposites. *Macromolecules* **2015**, *48*, 5433–5438.
- (8) Knauer, S. T.; Douglas, J. F.; Starr, F. W. The Effect of Nanoparticle Shape on Polymer–Nanocomposite Rheology and Tensile Strength. *J. Polym. Sci., Part B: Polym. Phys.* **2007**, *45*, 1882–1897.
- (9) Chevigny, C.; Dalmás, F.; Di Cola, E.; Gígenes, D.; Bertin, D.; Boué, F. o.; Jestin, J. Polymer-Grafted-Nanoparticles Nanocomposites: Dispersion, Grafted Chain Conformation, and Rheological Behavior. *Macromolecules* **2010**, *44*, 122–133.
- (10) Starr, F. W.; Schröder, T. B.; Glotzer, S. C. Molecular Dynamics Simulation of a Polymer Melt with a Nanoscopic Particle. *Macromolecules* **2002**, *35*, 4481–4492.
- (11) Zhu, A.-J.; Sternstein, S. S. Nonlinear Viscoelasticity of Nanofilled Polymers: Interfaces, Chain Statistics and Properties Recovery Kinetics. *Compos. Sci. Technol.* **2003**, *63*, 1113–1126.
- (12) Krutyeva, M.; Wischniewski, A.; Monkenbusch, M.; Willner, L.; Maiz, J.; Mijangos, C.; Arbe, A.; Colmenero, J.; Radulescu, A.; Holderer, O. Effect of Nanoconfinement on Polymer Dynamics: Surface Layers and Interphases. *Phys. Rev. Lett.* **2013**, *110*, 108303.
- (13) Li, Y.; Tao, P.; Viswanath, A.; Benicewicz, B. C.; Schädler, L. S. Bimodal Surface Ligand Engineering: The Key to Tunable Nanocomposites. *Langmuir* **2013**, *29*, 1211–1220.
- (14) Nodoro, T. V.; Böhm, M. C.; Müller-Plathe, F. Interface and Interphase Dynamics of Polystyrene Chains near Grafted and Ungrafted Silica Nanoparticles. *Macromolecules* **2012**, *45*, 171–179.
- (15) Moll, J. F.; Akcora, P.; Rungta, A.; Gong, S.; Colby, R. H.; Benicewicz, B. C.; Kumar, S. K. Mechanical Reinforcement in Polymer Melts Filled with Polymer Grafted Nanoparticles. *Macromolecules* **2011**, *44*, 7473–7477.
- (16) Senses, E.; Faraone, A.; Akcora, P. Microscopic Chain Motion in Polymer Nanocomposites with Dynamically Asymmetric Interphases. *Sci. Rep.* **2016**, *6*, 29326.
- (17) Senses, E.; Akcora, P. An Interface-Driven Stiffening Mechanism in Polymer Nanocomposites. *Macromolecules* **2013**, *46*, 1868–1874.
- (18) Gao, H.; Matyjaszewski, K. Synthesis of Functional Polymers with Controlled Architecture by Crp of Monomers in the Presence of Cross-Linkers: From Stars to Gels. *Prog. Polym. Sci.* **2009**, *34*, 317–350.
- (19) Ren, J. M.; McKenzie, T. G.; Fu, Q.; Wong, E. H. H.; Xu, J.; An, Z.; Shanmugam, S.; Davis, T. P.; Boyer, C.; Qiao, G. G. Star Polymers. *Chem. Rev.* **2016**, *116*, 6743–6836.
- (20) Kapnistos, M.; Lang, M.; Vlassopoulos, D.; Pyckhout-Hintzen, W.; Richter, D.; Cho, D.; Chang, T.; Rubinstein, M. Unexpected Power-Law Stress Relaxation of Entangled Ring Polymers. *Nat. Mater.* **2008**, *7*, 997–1002.
- (21) Vlassopoulos, D.; Fytas, G.; Pakula, T.; Roovers, J. Multiarm Star Polymers Dynamics. *J. Phys.: Condens. Matter* **2001**, *13*, R855.
- (22) Daniel, W. F.; Burdyńska, J.; Vatankeh-Varnoosfaderani, M.; Matyjaszewski, K.; Paturej, J.; Rubinstein, M.; Dobrynin, A. V.; Sheiko, S. S. Solvent-Free, Supersoft and Superelastic Bottlebrush Melts and Networks. *Nat. Mater.* **2016**, *15*, 183–189.
- (23) Shchetnikava, V.; Slot, J. J. M.; van Ruymbeke, E. A Comparison of Tube Model Predictions of the Linear Viscoelastic Behavior of Symmetric Star Polymer Melts. *Macromolecules* **2014**, *47*, 3350–3361.
- (24) Chremos, A.; Douglas, J. F. Communication: When Does a Branched Polymer Become a Particle? *J. Chem. Phys.* **2015**, *143*, 111104.
- (25) Yurekli, K.; Karim, A.; Amis, E. J.; Krishnamoorti, R. Phase Behavior of Ps–Pvme Nanocomposites. *Macromolecules* **2004**, *37*, 507–515.
- (26) Hammouda, B. Sans from Homogeneous Polymer Mixtures: A Unified Overview. In *Polymer Characteristics*; Springer Berlin Heidelberg: Berlin, Heidelberg, 1993; pp 87–133.
- (27) Colmenero, J.; Arbe, A. Segmental Dynamics in Miscible Polymer Blends: Recent Results and Open Questions. *Soft Matter* **2007**, *3*, 1474–1485.
- (28) Tyagi, M.; Arbe, A.; Colmenero, J.; Frick, B.; Stewart, J. Dynamic Confinement Effects in Polymer Blends. A Quasielastic Neutron Scattering Study of the Dynamics of Poly (Ethylene Oxide) in a Blend with Poly (Vinyl Acetate). *Macromolecules* **2006**, *39*, 3007–3018.
- (29) Lorthioir, C.; Alegría, A.; Colmenero, J. Out of Equilibrium Dynamics of Poly (Vinyl Methyl Ether) Segments in Miscible Poly (Styrene)-Poly (Vinyl Methyl Ether) Blends. *Phys. Rev. E: Stat. Phys., Plasmas, Fluids, Relat. Interdiscip. Top.* **2003**, *68*, 031805.
- (30) Milner, S.; McLeish, T.; Young, R.; Hakiki, A.; Johnson, J. Dynamic Dilution, Constraint-Release, and Star–Linear Blends. *Macromolecules* **1998**, *31*, 9345–9353.
- (31) Shivokhin, M.; Van Ruymbeke, E.; Bailly, C.; Kouloumasis, D.; Hadjichristidis, N.; Likhtman, A. E. Understanding Constraint Release in Star/Linear Polymer Blends. *Macromolecules* **2014**, *47*, 2451–2463.
- (32) Arbe, A.; Pomposo, J. A.; Asenjo-Sanz, I.; Bhowmik, D.; Ivanova, O.; Kohlbrecher, J.; Colmenero, J. Single Chain Dynamic Structure Factor of Linear Polymers in an All-Polymer Nano-Composite. *Macromolecules* **2016**, *6*, 2354–2364.
- (33) Tuteja, A.; Duxbury, P. M.; Mackay, M. E. Polymer Chain Swelling Induced by Dispersed Nanoparticles. *Phys. Rev. Lett.* **2008**, *100*, 077801.
- (34) Daoud, M.; Cotton, J. Star Shaped Polymers: A Model for the Conformation and Its Concentration Dependence. *J. Phys. (Paris)* **1982**, *43*, 531–538.
- (35) Lodge, T. P.; McLeish, T. C. Self-Concentrations and Effective Glass Transition Temperatures in Polymer Blends. *Macromolecules* **2000**, *33*, 5278–5284.
- (36) Yang, H.; Shibayama, M.; Stein, R. S.; Shimizu, N.; Hashimoto, T. Deuteration Effects on the Miscibility and Phase Separation Kinetics of Polymer Blends. *Macromolecules* **1986**, *19*, 1667–1674.
- (37) Cendoya, I.; Alegría, A.; Alberdi, J.; Colmenero, J.; Grimm, H.; Richter, D.; Frick, B. Effect of Blending on the Pvme Dynamics. A Dielectric, Nmr, and Qens Investigation. *Macromolecules* **1999**, *32*, 4065–4078.
- (38) Leroy, E.; Alegría, A.; Colmenero, J. Quantitative Study of Chain Connectivity Inducing Effective Glass Transition Temperatures in Miscible Polymer Blends. *Macromolecules* **2002**, *35*, 5587–5590.
- (39) Powell, M. J. Site Percolation in Randomly Packed Spheres. *Phys. Rev. B: Condens. Matter Mater. Phys.* **1979**, *20*, 4194–4198.
- (40) Frick, B.; Richter, D. The Microscopic Basis of the Glass Transition in Polymers from Neutron Scattering Studies. *Science* **1995**, *267*, 1939–1945.

- (41) Roland, C. M.; Ngai, K. L. Segmental Relaxation and Molecular Structure in Polybutadienes and Polyisoprene. *Macromolecules* **1991**, *24*, 5315–5319.
- (42) Holt, A. P.; Bocharova, V.; Cheng, S.; Kisiuk, A. M.; Ehlers, G.; Mamontov, E.; Novikov, V. N.; Sokolov, A. P. Interplay between Local Dynamics and Mechanical Reinforcement in Glassy Polymer Nanocomposites. *Phys. Rev. Mater.* **2017**, *1*, 062601.
- (43) Böhmer, R.; Ngai, K.; Angell, C.; Plazek, D. Nonexponential Relaxations in Strong and Fragile Glass Formers. *J. Chem. Phys.* **1993**, *99*, 4201–4209.
- (44) Richter, D.; Monkenbusch, M.; Arbe, A.; Colmenero, J. Neutron Spin Echo in Polymer Systems. In *Neutron Spin Echo in Polymer Systems*; Springer Berlin Heidelberg: Berlin, Heidelberg, 2005; pp 1–221.
- (45) Arbe, A.; Pomposo, J. A.; Asenjo-Sanz, I.; Bhowmik, D.; Ivanova, O.; Kohlbrecher, J.; Colmenero, J. Single Chain Dynamic Structure Factor of Linear Polymers in an All-Polymer Nano-Composite. *Macromolecules* **2016**, *49*, 2354–2364.
- (46) de Gennes, P.-G. Reptation of a Polymer Chain in the Presence of Fixed Obstacles. *J. Chem. Phys.* **1971**, *55*, 572.
- (47) Li, Y.; Kröger, M.; Liu, W. K. Nanoparticle Effect on the Dynamics of Polymer Chains and Their Entanglement Network. *Phys. Rev. Lett.* **2012**, *109*, 118001.
- (48) Schwahn, D.; Pipich, V.; Richter, D. Composition and Long-Range Density Fluctuations in Peo/Pmma Polymer Blends: A Result of Asymmetric Component Mobility. *Macromolecules* **2012**, *45*, 2035–2049.
- (49) Fernandes, A.; Barlow, J.; Paul, D. Blends Containing Polymers of Epichlorohydrin and Ethylene Oxide. Part I: Polymethacrylates. *J. Appl. Polym. Sci.* **1986**, *32*, 5481–5508.
- (50) Loppinet, B.; Stiakakis, E.; Vlassopoulos, D.; Fytas, G.; Roovers, J. Reversible Thermal Gelation in Star Polymers: An Alternative Route to Jamming of Soft Matter. *Macromolecules* **2001**, *34*, 8216–8223.
- (51) Senses, E.; Narayanan, S.; Mao, Y.; Faraone, A. Nanoscale Particle Motion in Attractive Polymer Nanocomposites. *Phys. Rev. Lett.* **2017**, *119*, 237801.
- (52) Liu, X.; Jin, X.; Ma, P. X. Nanofibrous Hollow Microspheres Self-Assembled from Star-Shaped Polymers as Injectable Cell Carriers for Knee Repair. *Nat. Mater.* **2011**, *10*, 398.
- (53) Hadjichristidis, N.; Pitsikalis, M.; Iatrou, H.; Driva, P.; Sakellariou, G.; Chatzichristidi, M. *6.03-Polymers with Star-Related Structures: Synthesis, Properties, and Applications*; Elsevier: Amsterdam, 2012; pp 29–111.
- (54) Kline, S. Reduction and Analysis of SANS and USANS Data Using Igor Pro. *J. Appl. Crystallogr.* **2006**, *39*, 895–900.
- (55) Meyer, A.; Dimeo, R.; Gehring, P.; Neumann, D. The High-Flux Backscattering Spectrometer at the NIST Center for Neutron Research. *Rev. Sci. Instrum.* **2003**, *74*, 2759–2777.
- (56) Azuah, R. T.; Kneller, L. R.; Qiu, Y.; Tregenna-Piggott, P. L.; Brown, C. M.; Copley, J. R.; Dimeo, R. M. Dave: A Comprehensive Software Suite for the Reduction, Visualization, and Analysis of Low Energy Neutron Spectroscopic Data. *J. Res. Natl. Inst. Stand. Technol.* **2009**, *114*, 341–358.